Journal of Materials Science: Materials in Engineering

ORIGINAL PAPER

Open Access

Fabrication and evaluation of a 3D decellularized-plant scaffold modified with composite hydrogel for bone tissue engineering

Mahsa Abbasi[1,2,3†], Parisa Sahami Gilan[2,3†], Maryam Zandian[2,3], Ghazal Sanjabi[2,3], Soroor Sadegh Malvajerd[3,4], Gholamreza Bahrami[5], Mohammad Reza Khirehgesh[2,3], Hossein Derakhshankhah[2,3], Zahra Pourmanouchehri[2,3] and Zhila Izadi[2,3*]

Abstract

Objective Three-dimensional (3D) decellularized scaffolds, providing Supportive matrices for cell growth and tissue regeneration, have gained attention as promising methods in tissue engineering and regenerative medicine. It has been established that plants are more dependable sources than animal tissues. Among various plant species, Aloe Vera stands out due to its biocompatibility and wound-healing properties, making it a viable candidate for sourcing 3D scaffolds. This study assessed the mechanical stability, drug release kinetics, and tissue integrity of decellularized Aloe Vera scaffolds coated with CMC.

Methods and materials Sodium dodecyl sulfate (SDS) facilitated the creation of 3D decellularized scaffolds from the Aloe Vera plant. Post-evaluation of the decellularized tissue, alendronate sodium (Aln), an osteogenic drug, was incorporated into the 3D scaffold via the wet impregnation method. An oligosaccharide derived from Rosa Canina was added to Aln, serving as an agent to promote cell proliferation and differentiation. To improve mechanical stability and ensure a sustained release of alendronate sodium, the decellularized scaffolds were coated with carboxymethyl cellulose (CMC) hydrogel in 1% and 2% containing the drug.

Results The decellularization process underwent optimization, resulting in improved physicochemical characteristics of the scaffolds. Incorporating alendronate sodium, oligosaccharide, and hydrogel coating, on the one hand, increased the swelling capacity, mechanical strength, and reduced the degradation time of the scaffold, and on the other hand, provided a controlled drug release mechanism. Also, this group exhibited suitable compatibility with cells and blood, and an increase in the migration and proliferation of MG63 cells was noted within the modified scaffolds.

Conclusion These findings Suggest that the 3D decellularized scaffold, which incorporates Aln and oligosaccharides with a CMC hydrogel coating, offers a fresh outlook for future research in bone tissue engineering and holds significant potential for clinical use.

†Mahsa Abbasi and Parisa Sahami Gilan made equal contribution to this work.

*Correspondence:
Zhila Izadi
izadi.zhila@yahoo.com; Zhila.izadi@gmail.com
Full list of author information is available at the end of the article

© The Author(s) 2025. **Open Access** This article is licensed under a Creative Commons Attribution 4.0 International License, which permits use, sharing, adaptation, distribution and reproduction in any medium or format, as long as you give appropriate credit to the original author(s) and the source, provide a link to the Creative Commons licence, and indicate if changes were made. The images or other third party material in this article are included in the article's Creative Commons licence, unless indicated otherwise in a credit line to the material. If material is not included in the article's Creative Commons licence and your intended use is not permitted by statutory regulation or exceeds the permitted use, you will need to obtain permission directly from the copyright holder. To view a copy of this licence, visit http://creativecommons.org/licenses/by/4.0/.

Highlights

- The physicochemical properties and biocompatibility of a 3D decellularized plant scaffold can be a suitable candidate for bone tissue engineering application.
- The fabricated scaffolds have good potential for drug loading.
- Coating of the scaffolds with cellulose methylcellulose (CMC) controlled the release of Alendronate for a longer time.
- The presence of oligosaccharides in the scaffold structure induced the proliferation and migration of MG63 (osteoblast-like) cells.

Keywords 3D scaffolds, Decellularized tissue of the aloe vera plant, Carboxy methyl cellulose (CMC), Alendronate sodium (Aln), Oligosaccharide extracted from Rosa Canina

Graphical Abstract

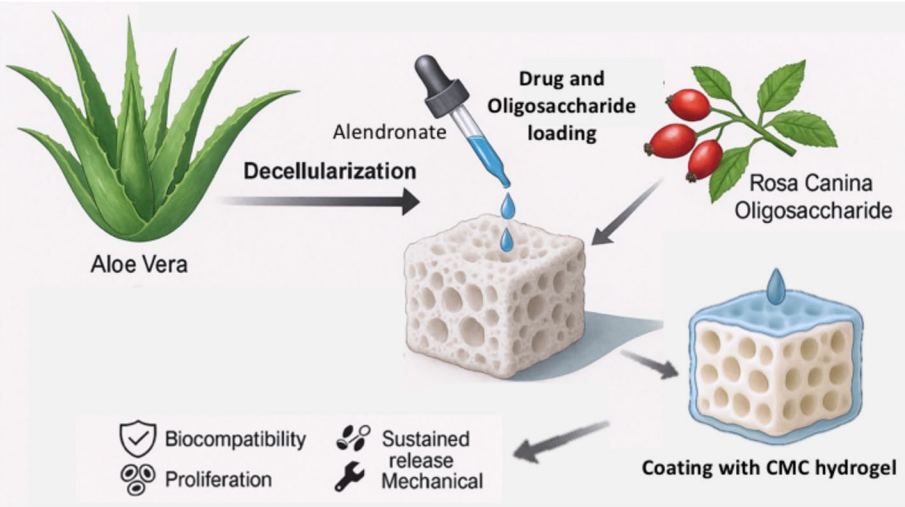

Introduction

Three-dimensional (3D) scaffolds are porous, biocompatible, and biodegradable structures that support cell growth by providing mechanical and biochemical cues within a biomimetic microenvironment (Loh and Choong 2013). In tissue engineering, they are widely applied in bone and cartilage repair, drug delivery, and cell behavior studies (Singh et al. 2022). Among the various materials explored for scaffold fabrication, decellularized tissues have emerged as effective alternatives due to their preserved extracellular matrix (ECM) architecture, which facilitates cell adhesion, proliferation, and differentiation (Urciuolo et al. 2018; Tohamy et al. 2018). Decellularized scaffolds can be derived from animal, human, or plant tissues (Wu et al. 2015). Plant-derived scaffolds are gaining attention due to their inherent structural diversity, widespread availability, and lower risk of zoonotic disease transmission (Contessi Negrini et al. 2020; Adhikari et al. 2023).

In particular, cellulose, a major component of plant tissues, offers excellent mechanical strength, porosity, and hydrophilicity, making it a suitable material for biomedical use (Iravani and Varma 2019; Arslan et al. 2023). Various plant species, including celery, apple, and Aloe vera, have been explored for scaffold development (Wang et al. 2020; Lee et al. 2019; Peter et al. 2010). Its biocompatibility and ability to support tissue regeneration make it a strong candidate for use in decellularized scaffolds. Several decellularization techniques using detergents, enzymes, or acids can be employed to remove cellular components while preserving ECM integrity. The effectiveness of these methods is typically evaluated via histology, biochemical assays, scanning electron microscopy (SEM), mechanical testing, and biocompatibility assessments (Gao et al. 2019). To further enhance scaffold functionality, therapeutic agents such as Alendronate sodium (Aln) a bisphosphonate known for promoting

bone regeneration and mineral density (Mutra et al. 2023). can be incorporated using techniques like wet impregnation. In this study, we combined Aln with oligosaccharides derived from Rosa canina, which exhibit antioxidant activity and stimulate cell proliferation and differentiation (J. Roelofs et al. 2010; Patel et al. 2012). Crosslinking and coating the scaffold with carboxymethyl cellulose (CMC) hydrogel improved mechanical stability and controlled drug release. CMC is a cost-effective, water-soluble polysaccharide widely used in tissue engineering due to its mechanical strength, hydrophilicity, and rheological properties (Ensrud et al. 1997; Black et al. 1996). The combination of Alendronate sodium (Aln) with bioactive compounds can enhance its regenerative efficacy. In this study, oligosaccharides derived from Rosa canina were incorporated into the Aln formulation as co-active agents. These low-molecular-weight carbohydrates exhibit strong antioxidant activity, promote mineral absorption, and stimulate cell proliferation and differentiation, making them valuable additives for scaffold activation (Li et al. 2021; Jia et al. 2022). To further improve scaffold integration and mechanical stability, both chemical and physical crosslinking techniques were employed (Whistler and BeMiller 2008); Khazaei et al. 2020; Sajadimajd et al. 2020) Coating the scaffold with suitable materials like hydrogels can further increase stability and mechanical strength while controlling drug release. One of the hydrogels used in this study was carboxymethyl cellulose (CMC), a water-soluble linear polysaccharide derived from abundantly available ethylene glycol (Zhang et al. 2022; Tarafder and Bose 2014; Heinze and Pfeiffer 1999).This hydrogel is favored in tissue engineering and medical applications due to its simple and cost-effective synthesis (Su et al. 2010; Rosilio et al. 2000), formability (Roy and Rhim 2020; Kadokawa et al. 2012), excellent formability, good mechanical strength (Kadokawa et al. 2012), beneficial rheological properties (Gregorova et al. 2015), hydrophilicity (Benslimane et al. 2016), and notable viscosity (Parikh et al. 2003).

This study involved the ionic and non-ionic decellularization of Aloe vera plant tissue, with an evaluation of the decellularization quality. To enhance cell proliferation, Aln and oligosaccharides from Rosa canina were incorporated into these decellularized scaffolds. Following this, the scaffolds were coated with a CMC hydrogel to evaluate their flexibility, mechanical properties, and drug-controlled release capabilities. The effectiveness of these plant-based scaffolds, enriched with active components, was then assessed for their ability to induce cell migration, and they were recommended for bone tissue repair.

Materials and methods

Aloe Vera, Alendronate sodium (Sigma- Aldrich), EDTA (Merck), SDS 0.1% (Spectrum chemical), Triton X-100 (Sigma- Aldrich), Whitex, 70% Ethanol (Merck), PBS, Carboxy methyl cellulose (CMC) (Sigma- Aldrich), Oligosaccharide, 80% Isopropanol (Merck), Citric acid (CA), NaCl 1.2 M, Chloroform (Sigma- Aldrich), Acetone (Sigma- Aldrich), Tris-Base (Sigma- Aldrich), Liquid nitrogen, DMEM-F12 (Sigma- Aldrich), Fetal Bovine Serum (FBS) (GIBCO- USA), MTT (Sigma–Aldrich (USA).

Fabrication of plant-based 3D scaffolds: decellularization process

Fresh Aloe Vera leaves were purchased and stored at a temperature of 4°C. The leaves were halved, and the gel was carefully and completely extracted. To assess the cellulose structure on a microscopic scale, the leaves were sliced into pieces with radii of 1.5 cm and 3.5 cm using two different-sized punches.

Initially, the slices were immersed in a 0.1% (w/v) SDS solution and stirred on a magnetic stirrer at 70 rpm at 25 °C for 4 h. After thorough rinsing with distilled water, a mixture of 10 ml of bleach and 1 ml of Triton X100 was prepared, with the total volume adjusted to 100 ml. The leaves were then soaked in this solution for 12 h while being stirred at the same speed. Following this, they underwent multiple washes with distilled water before being immersed in 70% ethanol for 1 h. The samples were again washed, soaked in PBS buffer for one hour on a magnetic mixer, and rinsed once more. Lastly, the 3D decellularized scaffolds were stored in a freezer at −20 °C overnight for freeze-drying (Yang and Zhu 2007).

DNA content analysis and protein assessment

The NanoDrop technique was utilized to determine the presence of protein within decellularized plant tissue. This method involves the sample evaporating and forming a liquid column due to surface tension between the ends of an optical fiber (Zahmati et al. 2017). The 3D decellularized scaffold of the Aloe Vera plant, along with fresh Aloe Vera tissue, was powdered using Liquid nitrogen. A solution of 1.5 ml of 1% TCA/acetone (w/v) was added to each sample; these were then vortexed, incubated for one minute, and centrifuged for ten minutes at 4°C. After discarding the supernatant, acetone was used to wash the sediment, which was then incubated and centrifuged again (Desjardins et al. 2009). The sediments were dissolved in distilled water, and their absorbance at 280 nm was evaluated with the NanoDrop device. DNA from both fresh and dried plant leaves was assessed through PCR-based genetic analysis, with concentration

determinations made using a Victor 3 spectrophotometer (Perkin Elmer, Waltham, MA). Following freeze-drying, both the 3D decellularized scaffold and fresh plant tissue were powdered with Liquid nitrogen in a ceramic mortar. Two 50 ml Falcon tubes were prepared, each containing 30 ml of CTAB buffer. Ten grams of powder from the decellularized Aloe Vera scaffold was placed in one tube, while 10 g from the fresh tissue went into the other. Each Falcon tube was incubated at 60 °C for 2 to 4 h and Subsequently centrifuged at ambient temperature for 5 min at 3000 rpm. The Supernatant was divided into 2 ml microtubes, incubated for 15 min at 60 °C, and transferred to new microtubes with 600 µl chloroform. After vortexing and centrifugation, 1 ml of CTAB precipitation solution was added and allowed to incubate for 1 h at room temperature. The Supernatant was discarded; 500 µl of 1.2 M NaCl solution was added to the residue, and the sediments were completely dissolved by pipetting. The samples were then treated with 500 µl of chloroform and centrifuged. The upper phase was separated into another microtube, followed by the addition of 0.6 volume of 80% isopropanol, which was incubated and centrifuged. After discarding the Supernatant, 500 µl of ethanol was added to the sediments, mixed slowly, centrifuged again (Rodrigues et al. 2012) and finally, 20 µl of distilled water was added before storing the samples at −20°C. The DNA quantity was ultimately evaluated with a NanoDrop device by measuring absorption at 260 nm (Rosilio et al. 2000; Roy and Rhim 2020).

Loading the alendronate sodium and oligosaccharide on the decellularized scaffolds

At this step, the decellularized scaffolds were arranged in a plate, and sodium alendronate (Aln) along with oligosaccharide was measured in identical proportions of 20, 40, and 80 mg. These components were applied to the scaffolds using the wet saturation technique. Following this process, the scaffolds were allowed to dry at room temperature overnight (Fig. 1).

Coating scaffolds with carboxymethyl cellulose (CMC)-based hydrogel

Carboxymethyl cellulose solutions at concentrations of 1% and 2% were prepared in separate flasks. Equal ratios (15, 20, and 25) of Aln and oligosaccharide were measured and added to each flask. These mixtures were then stirred on a magnetic stirrer for 1 h until thoroughly combined. Subsequently, 0.5% citric acid was incorporated to cross-link the carboxymethyl cellulose. The resulting scaffolds from this process were then immersed in hydrogels for a duration of 2 h. Finally, they were left to dry at room temperature (Table 1 and Fig. 1).

Chemical, physical, and mechanical characterizations

Fourier transform infrared spectrometer (FT-IR)

FT-IR device with Nicolet 170-SX model (Thermo Nicolet Ltd., USA) technique was used to identify functional groups and examine the bonds created between scaffolds loaded with Aln/oligosaccharide and hydrogel scaffolds

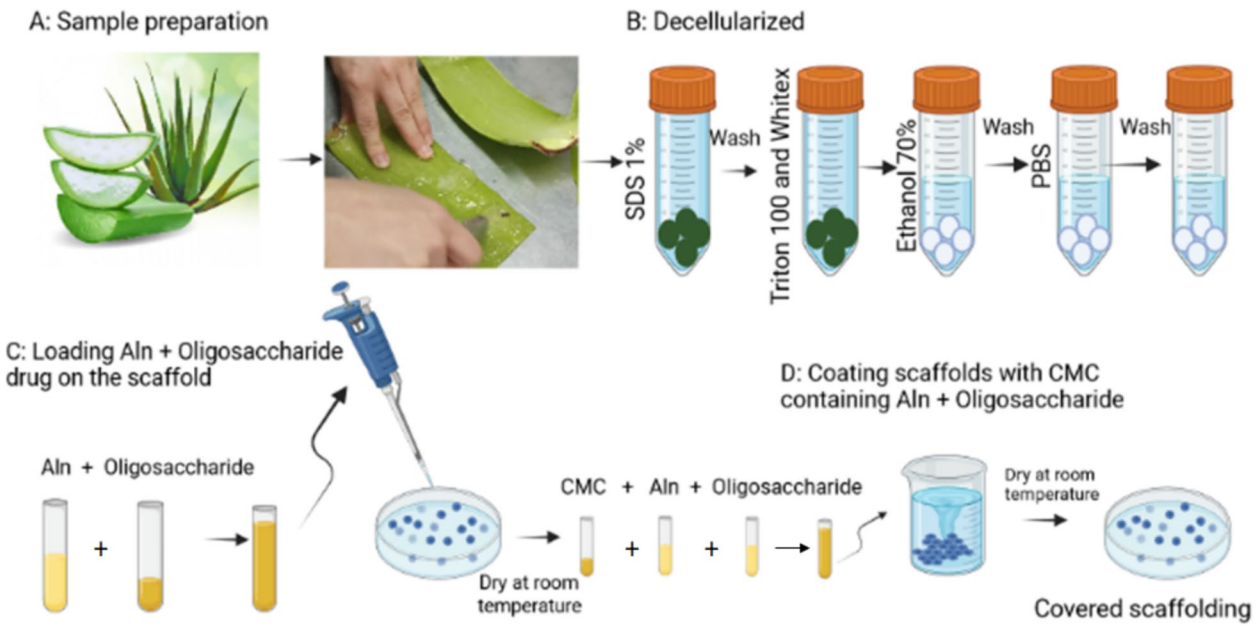

Fig. 1 Decellularization method and preparation of scaffolds with carboxymethyl cellulose (CMC) hydrogel coating containing alendronate sodium (Aln) and oligosaccharide

Table 1 The ratio of alendronate sodium (AS), oligosaccharide, and hydrogel for the preparation of AS and oligosaccharide loaded scaffold and hydrogel-coated scaffold containing AS and oligosaccharide

Loading the drug on the scaffold		Coating the scaffolds with hydrogel		
Groups	Aln and Oligosaccharide (mg)	CMC (%)	Aln (mg)	Oligosaccharide (mg)
a	20	2	15	15
b	40	2	20	20
c	**80**	**2**	**25**	**25**
d	20	1	15	15
e	40	1	20	20
f	80	1	25	25

CMC Cellulose methylcellulose

(CMC) containing Aln/oligosaccharide. It should be noted that the range of wave numbers was from 100 to 4000 cm^{-1} (Riswahyuli et al. 2020).

Swelling ratio studies

At first, decellularized scaffolds, scaffolds containing Aln and oligosaccharides, and scaffolds with and without hydrogel coating were in petri dishes using an analytical balance (GCL603i, A&D Weighing, Germany). Then, wet scaffolds were placed at different times to reach the saturation value. Simultaneously, the swelling percentage of the scaffolds was calculated. The swelling ratio (Sg/g) and water retention percentage were determined using the following Eqs. (Bilezikian et al. 2008).

$$\text{Swelling ratio}\left(S_{g/g}\right) = \frac{W_t - W_0}{W_0} \tag{1-2}$$

$$\text{Water retention}\ (\%) = \frac{W_t - W_0}{W_d - W_0} \tag{2-2}$$

W_O, the initial weight of scaffolds; W_t, the weight of scaffolds after being placed in PBS at different time intervals; W_d, the initial weight of swollen scaffolds.

Biodegradability study

To check the biodegradability of the scaffolds, first, the decellularized scaffolds, scaffolds containing Aln/oligosaccharides, and scaffolds coated with hydrogel (CMC/Aln/oligosaccharides) were weighed, and the initial weight was recorded. Then the scaffolds were immersed in PBS buffer and placed in the germinator at 37 °C for different periods (1, 2, 3, and 4 weeks). The existing PBS buffer was replaced with fresh PBS solution every week (Morris et al. 2017).

(3-2)

$$weight.loss\ (\%) = \frac{(W_t - W_0)}{W_0} \tag{3-2}$$

W_O, the initial weight of scaffolds, and W_t, the weight of scaffolds after being placed in PBS solution (pH = 7.4).

Mechanical properties

Decellularized scaffolds, Aln/oligosaccharide loaded scaffolds, and hydrogel-coated scaffolds (CMC/Aln-oligosaccharides) were tested for mechanical properties using a closed-loop control testing machine (800LE3/2, Testing Resources Inc. MN, USA) at a deformation rate of 0.05 mm/s in 1 × 3 dimensions were prepared. The discs were compressed to 50% of their initial thickness and then deflated to determine their elastic decomposition capacity. The elastic modulus of each structure was calculated from the slope of the stress–strain curve between 75 and 100% stress during the loading phase (Aoki and Ajiro 2017).

Drug release assay

The release rate of the drug (alendronate sodium) in scaffolds containing Aln/oligosaccharide with and without hydrogel coating was measured using the Franz cell and Hanon FC1200/FC1500 laboratory circulator.

Scaffolds with a radius of 3 cm were cut and placed in the Franz's cell for 72 h. PBS was poured into the Franz cell, and at different time points, 2 ml of the liquid inside Franz's cell containing drugs (Aln in PBS) was removed and replaced with fresh PBS. Stock solution 1: Fe^{3+} (27 mg) was weighed and dissolved in a solution (3.5 ml of perchloric acid and 6.5 ml of distilled water) and made to a final volume of 20 ml. Stock solution 2: Aln (27 mg) was weighed and dissolved again, and the volume was brought to 20 ml. Acid and water solution: 3.5 ml of perchloric acid was added to 16.5 ml of distilled water to achieve a total volume of 20 ml (Riswahyuli et al. 2020). To evaluate the drug release kinetics, experimental release data obtained from both hydrogel-coated and uncoated scaffolds were fitted to four conventional mathematical models: zero-order, first-order, Higuchi, and Korsmeyer-Peppas. Data fitting was performed using linearized forms of each model, and the kinetic parameters (e.g., release rate constant k, release exponent n), as well as statistical metrics including the coefficient of determination (R^2), sum of squared errors (SSE), regression sum of squares (SSR), total sum of squares (SST), and mean percent error (%E), were calculated to assess the goodness of fit. The best-fitting model was selected based on the highest R^2 and lowest SSE and %E values.

Morphological study

To evaluate the structural architecture, scaffolds loaded with Aln/oligosaccharide, both with and without hydrogel coating, were analyzed using a morphology imaging method with a scanning electron microscope (SEM model (JSM-840A, JEOL)). Surface porosity was measured using optical interferometers (Accura 2000, Intekplus, Seoul, Korea) with a measurement area of 80 × 80 square micrometers. The results were averaged for each set. The scanning electron microscope can capture images of Surfaces with a magnification range of 10 to 500,000 nm (Jayaramudu et al. 2019). The designed 3D scaffolds were also averaged for each sample set.

Biocompatibility study

Hemo compatibility evaluation

About 8 ml of fresh blood was poured into tubes containing potassium oxalate anticoagulant (CBC) using venipuncture from different groups of decellularized scaffolds. Scaffolds containing Aln and oligosaccharides with and without hydrogel were prepared and poured into 2 ml microtubes for each group. There were two controls: the negative control included 200 ml diluted blood with PBS and the positive control included 200 ml diluted blood with distilled water. Then, 200 ml of diluted blood with PBS was added to the samples. All samples were incubated at 37 °C for 2 h. After centrifugation at 1000 rpm for 10 min, the Supernatant absorption was measured at a wavelength of 545 nm. The hemolysis (HP) percentage was calculated using the following Eqs. (Kim et al. 2022).

$$Hemolysis = \frac{Ct - Cnc}{Cpc - Cnc} \times 100 \quad (4\text{-}2)$$

C_t, the average of samples; Cnc, negative control; and C_{pc}, positive control.

Cell compatibility assessment on the osteoblast-like cells

The cell compatibility of the decellularized scaffolds on MG63 was assessed using the 3-(4, 5-dimethylthiazol-2-yl)−2, 5-diphenyltetrazolium bromide (MTT) method. Osteoblast-like cells were exposed to both modified and unmodified decellularized scaffolds carrying active substances (Aln and oligosaccharide) with coating to assess the cell survival and proliferation. The MG63 cells were planted in 96-well plates, at a density of 10^4 cells per well, and grown in culture media for 24 or 48 h. The Supernatant was removed and replaced with a 0.5 mg/ml MTT solution in RPMI 1640. Incubation with the samples, took 4 h under normal culture conditions. The media from each well was slowly removed, and the crystallized formazan dye was dissolved with 0.04 M HCl in absolute isopropanol and 1% dodecyl Sulfate. The optical density of the solution at 570 nm was determined using Multiscan Spectroscopy (Thermo Labsystems, Vantaa, Finland) and Ascent software (Thermo Labsystems, Vantaa, Finland) (Porebski et al. 1997).

Cell migration assay in vitro

Cell migration was determined with the aid of the cell scratch assay. MG63 cells were seeded into 24-well plates and allowed to grow until they nearly formed confluent monolayers. To exclude any effects from cell proliferation, cells were pretreated with the anti-proliferative agent mitomycin C (10 µg/L) for 2 h (Patel et al. 2012). A straight vertical scratch was made through the MG63 monolayers using a 1 ml plastic pipette tip. The cells were then cultured with the diluted scaffold extracts and the MG63 cell culture medium, respectively. The area was measured using a microscope equipped with a camera at 0 and 24 h. The space's area was measured using ImageJ. The cell migration rate was calculated according to the following equation: migration rate (%) = St/S0 × 100% (S0 initial hole area, St: cell covered area within the space at time t).

Statistical analysis

All data are presented as mean ± standard deviation (SD) from at least three independent experiments. Statistical analyses were performed using Microsoft Excel. For group comparisons, one-way ANOVA followed by unpaired two-tailed t-tests were applied where appropriate. Values of $p < 0.01$ (*) and $p < 0.01$ (**) were considered significant and very significant, respectively. Confidence intervals at 95% were calculated for key comparisons to support interpretation.

Results

Efficacy of decellularized plant-based scaffolds

SSR marker PCR amplification served as a quality assessment for genomic DNA extracted from Aloe Vera leaves. Clear DNA fragments were Successfully retrieved through PCR from fresh Aloe Vera leaves, confirmed via agarose gel electrophoresis. The DNA quantity in non-decellularized plant samples reached 514.9 ng, facilitated by a straightforward and non-toxic decellularization method for scaffolds. In contrast, the decellularized samples contained 2.1 ng/microliter of DNA. Ideally, the DNA content should not Surpass 50 ng per milligram of decellularized scaffold (Singh et al. 2022; Györgyey et al. 2013). The protein concentration in fresh plant tissue samples measured 1.46 mg/ml. Following the decellularization procedure, the protein level in the treated samples dropped to 0.29 mg/ml. This reduction to below 0.3 mg/ml signifies nearly complete purification of the plant tissue from cellular components and metabolites.

An approximately sevenfold decrease in protein content in the decellularized tissue compared to the original plant tissue highlights the effective purification process from cells and related metabolites (Fig. 2a, b).

Physical and mechanical properties

FT-IR results

In the cellulose scaffold/Aln drug spectrum, a shift in frequency from 958 cm^{-1} to 921 cm^{-1} was observed. This shift is attributed to the interaction between the P-O bond in alendronate sodium and OH groups in the cellulose scaffold. The C-O stretching frequency initially noted at 1062 cm^{-1} also displayed changes in intensity and frequency when compared to its presence in just the cellulose scaffold or the drug alone. Notably, the stretching bands at 952–1022 cm^{-1} and 923 cm^{-1} became more pronounced in the spectrum of the scaffold containing the drug Aln, highlighting the formation of P-O and P = O bonds between Aln and the cellulose scaffold, as depicted in their FT-IR spectrum.

According to Fig. 3, CMC, Aln, and oligosaccharides form hydrogen bonds with each other. In the combined CMC/Aln/oligosaccharides spectrum, a broad O–H stretching vibration band appears between 3234 and 2677 cm^{-1}, along with strong bending vibration bands at 1006 cm^{-1}. These are notably more intense than when CMC, Aln, or oligosaccharides are isolated. The shift to higher wavenumbers suggests hydrogen bond formation involving amino N–H and hydroxyl groups of Aln with CMC and oligosaccharides. These hydrogen bonds, particularly those between OH groups in cellulose scaffolds and the OH and NH bonds in alendronate sodium, as well as OH bonds in oligosaccharides, are visible around 3234 cm^{-1}. In the Aln/oligosaccharide spectrum, five hydrogen bonds were identified involving the oxygen of the Aln hydroxyl group with hydrogen atoms and Aln hydroxyl group. Additionally, hydrogen bonds were observed between the oxygen atoms of Aln phosphonate groups and OH groups of oligosaccharides, as well as Aln nitrogen atoms.

Swelling ratio

An essential aspect of plant scaffold technology is swelling. The 3D decellularization scaffolds demonstrated a

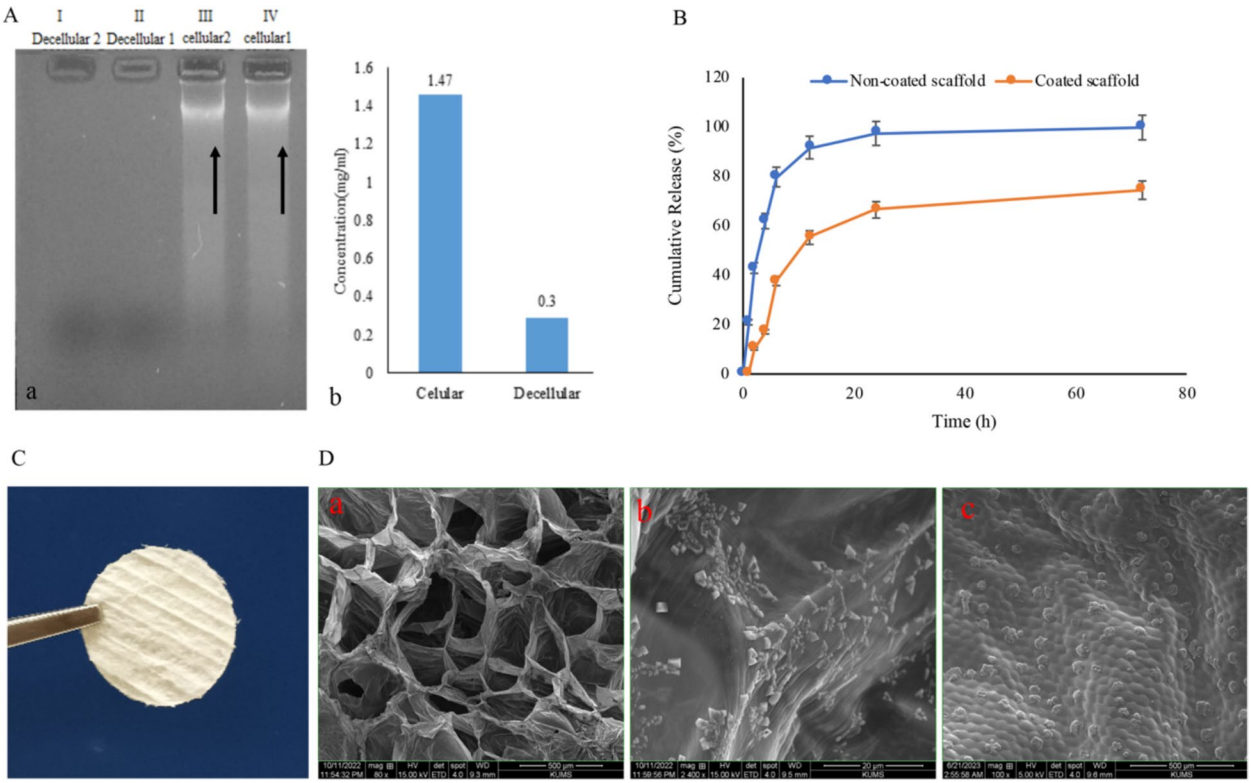

Fig. 2 **A** a) Decellularized Aloe Vera plant tissue free of any DNA (I and II), and presence of DNA in Aloe Vera plant tissue (III and IV). b) Measuring the amount of protein in cellular and decellularized groups. **B** In vitro culmative drug release profile of hydrogel-coated and non-coated scaffolds over 72 h. Data are presented as mean ± SD ($n = 3$) scaffolds coated with carboxymethyl cellulose (CMC) hydrogel containing AS and oligosaccharide. b) The inserts are Scaffolds loaded with Aln. **C** SEM a) Decellularized scaffold of Aloe Vera plant. b) Aln loaded on the decellularized scaffold of the Aloe Vera plant. c) CMC/Aln and oligosaccharide

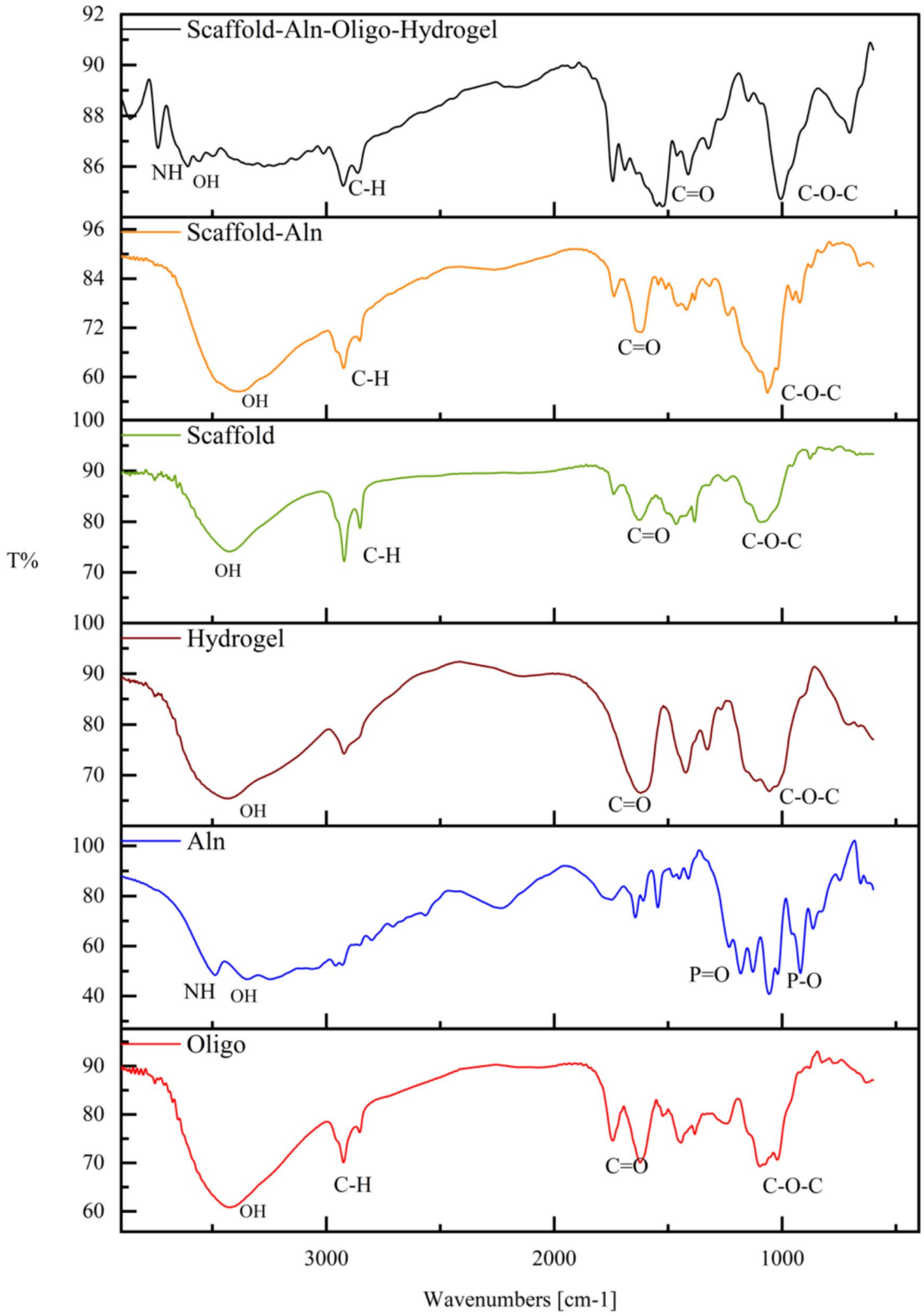

Fig. 3 FTIR results of Scaffold-Aln-Oligo-Hydrogel, Scaffold- Aln, Scaffold, Hydrogel, Aln, Oligo

significant capacity for swelling. Data shows that across all groups, swelling increased during the initial 6 h and subsequently decreased.

Degradation rate of scaffolds

Over 4 weeks, the degradability of decellularized scaffolds, as well as those containing Aln and oligosaccharide with and without hydrogel, experienced an accelerated rate. The findings suggest that the primary factor in the scaffold degradation is the hydrogel component (Fig. 4C).

Mechanical properties

The scaffold containing Aln and oligosaccharide demonstrated a mechanical strength of 9.12 MPa, while the scaffold lacking these components showed a lower strength of 5.49 MPa, attributed to hydrogen bonds formed between the scaffold, Aln, and oligosaccharide. As depicted in Fig. 4B, coating with hydrogel further increased the mechanical strength to 12.31 MPa. Enhancing the strength and elasticity of scaffolds is a notable advantage of these materials. Table 1 highlights an increase in flexibility at a concentration of 2% W/V. The mechanical strength improved by increasing the Aln and oligosaccharide ratio and shifting the hydrogel concentration from 1 to 2% W/V. However, it is crucial to note that at a hydrogel concentration of 1% W/V, the scaffold's mechaniFcal strength decreased with a higher Aln and oligosaccharide ratio (Fig. 4).

Controlled release kinetics of alendronate from decellularized scaffolds with and without hydrogel coating

The findings on swelling, degradation, and mechanical properties showed that the Aln/oligosaccharide (80 mg) and 2% CMC/Aln/oligosaccharide (25 mg) groups demonstrated the greatest resistance during the loading phase. Since alendronate sodium alone lacked an absorption spectrum, it was necessary to mix the release solutions with $FeCl_3$ solution. The absorbance of this newly formed complex was promptly measured at wavelengths of 290, 300, and 310 nm. A highly acidic

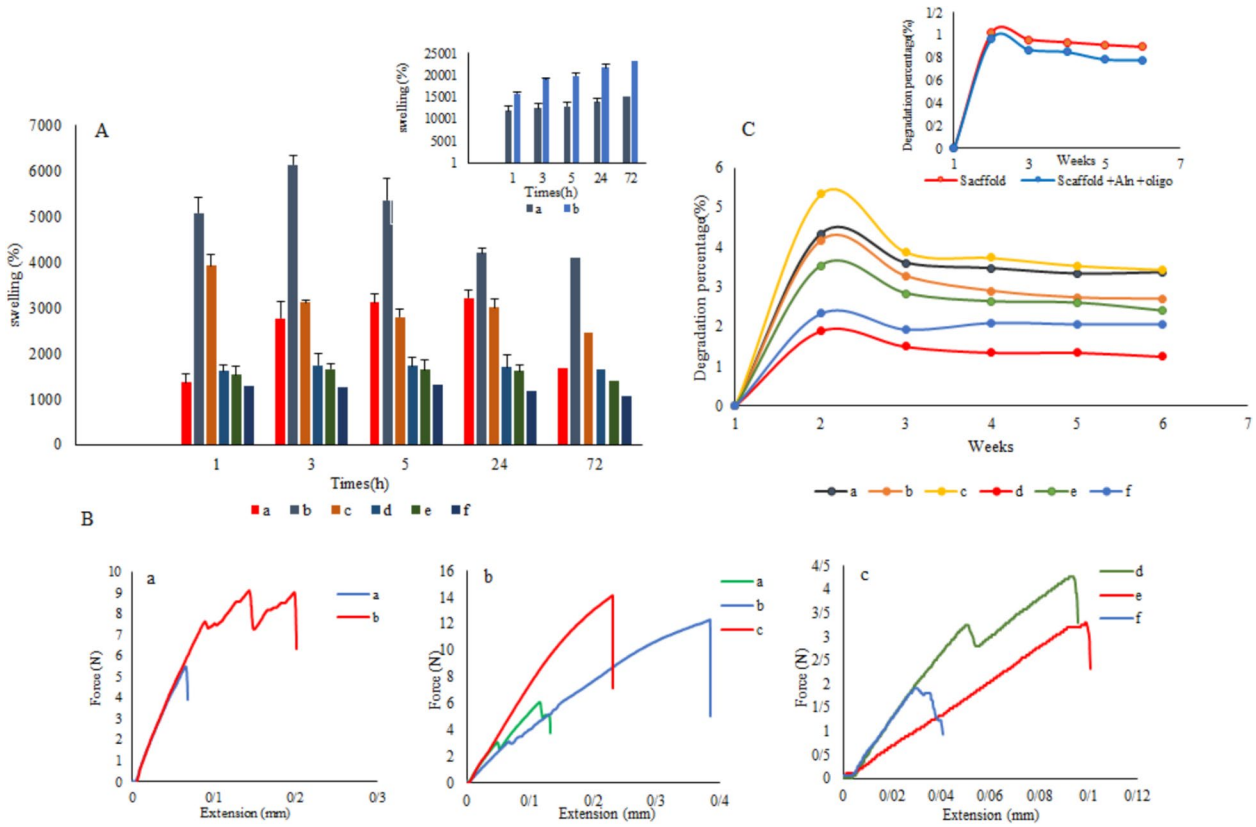

Fig. 4 **A** Swelling percentage in scaffolds coated with carboxymethyl cellulose (CMC) hydrogel containing AS and oligosaccharide in different ratios and concentrations. The inserts are scaffolds with and without AS and oligosaccharide. **B** Tensile strength a) Scaffolds without AS. b) Scaffolds loaded with AS. Scaffolds coated with a concentration of 2% W/V (CMC) containing AS and oligosaccharides with different ratios (Table 1 (a, b, c). c Scaffolds coated with a concentration of 1% W/V (CMC) containing Aln and oligosaccharide with different ratios in Table 1. **C** Degradability for scaffolds coated with hydrogel (CMC) with different concentrations containing Aln and oligosaccharide with different corresponding ratios (Table 1). The inserts are scaffolds without Aln and oligosaccharide-scaffolds loaded with Aln

environment was crucial to prevent the hydrolysis of Fe^{3+} ions. Within the 200 to 400 nm wavelength range, the absorption spectrum of the Fe^{3+} alendronate complex was recorded, with the complex itself and Fe^{3+} ions showing maximum absorbance at 260 and 238 nm, respectively.

The absorption spectrum of the acquired complex revealed that the uncoated scaffolds exhibited a faster release profile, characterized by an initial burst release. This phenomenon is commonly attributed to the rapid diffusion of drug molecules located near or on the scaffold Surface, with approximately 90.5% of the drug released within the first 12 h (Costa and Lobo 2001).

Conversely, hydrogel-coated scaffolds demonstrated a significantly slower and more controlled release, indicating that the hydrogel layer acts as a physical barrier modulating drug diffusion. Within the initial 12 h, approximately 63.2% of the drug is released (Fig. 2B). Hydrogels, due to their three-dimensional cross-linked polymer network, provide an additional diffusional resistance, thereby prolonging the release period and mitigating the burst effect (Peppas et al. 2000).

Among the four tested models, the Korsmeyer-Peppas model provided the best fit for both hydrogel-coated and uncoated scaffolds, as evidenced by the highest R^2 values (0.997 for uncoated and 0.992 for coated) and the lowest prediction errors, indicating that drug release in both systems is governed by a combination of diffusion and polymer matrix relaxation (Table 2). These findings align with previous reports highlighting the role of hydrogel coatings in achieving sustained and controlled drug delivery by regulating the mass transfer and matrix swelling. Overall, our results demonstrate that hydrogel coating effectively modulates scaffold release kinetics, making it a promising strategy for optimizing therapeutic efficacy and reducing initial burst release in scaffold-based drug delivery systems (Siepmann and Peppas 2012).

Morphological study

Scanning Electron Microscopy was employed to assess the quality of decellularization and maintain the structural integrity of the Aloe Vera plant after the process. The dimensional alterations in the 3D scaffolds were kept under 6%. Following the decomposition using the sodium dodecyl sulfate (SDS) protocol, the morphological structures and pore boundaries remained intact, ensuring the preservation of the plant tissue's original morphology with this method (Fig. 2C (a)). The morphology results in the scaffolds containing Aln and oligosaccharides in Fig. 2C. (b) show that Aln was loaded onto the decellularized scaffold of the Aloe Vera plant. The pores of the scaffold were found to be unchanged. In Fig. 2C (c). SEM images of hydrogel-coated scaffolds which showed that Aln crystals have irregular shapes and a wide size distribution.

Biocompatibility of plant-based scaffolds

Hemo compatibility results

Figure 5A presents the analysis results of the hemolytic rate for decellularized scaffolds and those incorporating Aln and oligosaccharide, both with and without hydrogel. The hemolysis ratio for the scaffold containing Aln and oligosaccharide at room temperature was significantly lower compared to the positive control ($P < 0.001$). Here, the positive control refers to blood lysed with water, while the negative control involves blood diluted with PBS.

The results of the cell compatibility investigation

The assessment of cell compatibility of modified decellularized scaffolds (with Aln and oligosaccharide) was conducted using the MTT method on MG63 cell lines. The findings indicated that MG63 cells maintained a Survival rate exceeding 90% over 24 and 48 h when exposed to scaffolds enhanced with Aln and oligosaccharide. This is in contrast to the control group, where cells were left

Table 2 Release parameters for the hydrogel-coated and non-coated scaffolds obtained after fitting data with different mathematical models of drug release kinetics

	Model	k	SSE	SSR	SST	R^2	%E
Non-coated	Zero-order	0.039	0.0073	0.23	0.25	0.916	6.7
	First-order	0.115	0.0021	0.24	0.25	0.974	3.9
	Higuchi	0.198	0.0005	0.25	0.25	0.994	1.9
	Korsmeyer-Peppas	0.263	0.0003	0.25	0.25	0.997	1.2
Coated	Zero-order	0.035	0.0056	0.23	0.26	0.930	6.2
	First-order	0.090	0.0024	0.25	0.26	0.970	4.1
	Higuchi	0.160	0.0011	0.25	0.26	0.985	3.1
	Korsmeyer-Peppas	0.205	0.0007	0.26	0.26	0.992	1.8

k Kinetic constant, *SSR* Sum square of regression, *SST* Sum square of total variation, *SSE* Sum square of errors, *R2* Coefficients of determination, *E%* Total error percent

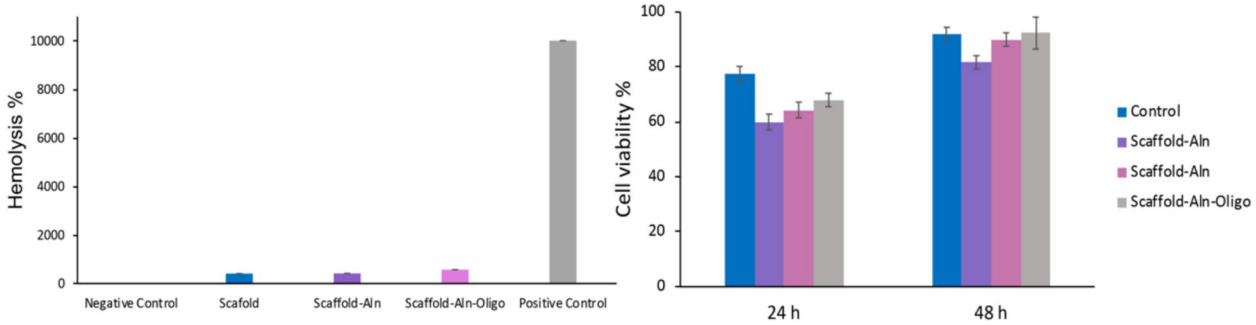

Fig. 5 Cell and blood compatibility; **A** Blood compatibility for coated and uncoated scaffolds containing alendronate sodium (Aln). $p < 0.001$(**) compared to positive control. Data are presented as mean ± SD ($n = 3$) **B** Cell compatibility result on MG63 cells; MTT of MG63 cells treated with coated and uncoated scaffolds after 24 and 48 h of incubation: $p < 0.01$ (*) in comparison to the control ($n = 3$). Migration of cells (assay for scratch wound healing): images were taken at 0, 12, and 24 h following wounding. Three separate experiments' worth of representative images are displayed, with dark areas denoting cell-deficient areas (wound area, ImageJ)

untreated, showing a statistically significant difference ($p < 0.05$), as illustrated in Fig. 5B.

Effects of the modified scaffolds on the cell migration

Figure 6 illustrates how modified scaffold extracts affect the migration of MG63 cells. After 24 h, all groups exhibited a significant number of migrated cells within the scratch areas. The control group showed a dispersed arrangement of cells that lacked substantial interactions, indicating single-cell migration patterns. In contrast, those treated with scaffold-Aln and scaffold-Aln and oligosaccharide extracts demonstrated collective movement in a sheet-like structure where most cells maintained their intercellular connections (Fig. 6, mean ± standard errors, $^*p < 0.01$). These scaffolds promoted cell growth and proliferation and were found to be safe and non-cytotoxic when applied within the body, effectively encouraging cellular growth and proliferation.

Discussion

In tissue engineering, the architecture of decellularized scaffolds is critical, as it replicates the natural extracellular matrix (ECM), facilitating nutrient diffusion, cell adhesion, and proliferation (Richbourg et al. 2019; Bickhard 2013). Decellularized tissues provide a 3D framework and native biochemical cues that support cellular functions essential for tissue regeneration (Wang et al. 2020; Modulevsky et al. 2014). Although animal-derived scaffolds are commonly used, they carry risks of immunogenicity and disease transmission. As an alternative, plant-derived scaffolds are renewable, accessible, and cost-effective, with diverse morphologies that can be leveraged for customized scaffold design (Mohammadinejad et al. 2016; Hickey and Pelling 2019).

This study evaluated Aloe vera as a plant-based scaffold source. Sodium dodecyl sulfate (SDS) was effective for decellularization, confirmed by reductions in DNA and protein content. The process preserved the plant's morphological structure and porosity while minimizing damage to the cellulose matrix (Ibrahim et al. 2020; Elliott and Robinson 1957). Alendronate (Aln), a bisphosphonate with osteogenic potential, was subsequently incorporated, along with oligosaccharides known for their bioactivity in promoting bone regeneration (Shin et al. 2021).

Aln and oligosaccharides were loaded into the Aloe vera scaffold using controlled release techniques. Carboxymethyl cellulose (CMC), a widely used biocompatible polymer, served as the hydrogel matrix. CMC enhances drug delivery, mechanical stability, and cell–scaffold interactions due to its tunable properties and water retention capacity (Ibrahim et al. 2020). However, its low mechanical strength requires optimization, which was addressed by incorporating shape-specific drug components and structural modifiers (Elliott and Robinson 1957; Surowiec et al. 2022).

FTIR analysis confirmed hydrogen bonding between hydroxyl groups in the scaffold and functional groups in Aln and oligosaccharides, suggesting stable integration. Water content plays a critical role in mechanical behavior; excessive hydration can reduce bone mineral density and strength (Euw et al. 2018). Our hydrogel scaffold exhibited high swelling capacity, peaking at 6 h, with limited expansion thereafter—likely due to the gel's structural limitations or saturation dynamics (Vyalikh et al. 2017; Pan et al. 2016). Given that reduced bone strength is a hallmark of conditions such as osteoporosis, scaffold designs must promote both mechanical integrity and biological performance (Hoshino et al. 2018; Ansari 2019).

The mechanical strength and degradation rate of the hydrogels were influenced by Aln and oligosaccharide ratios and hydrogel concentration. Gradual degradation

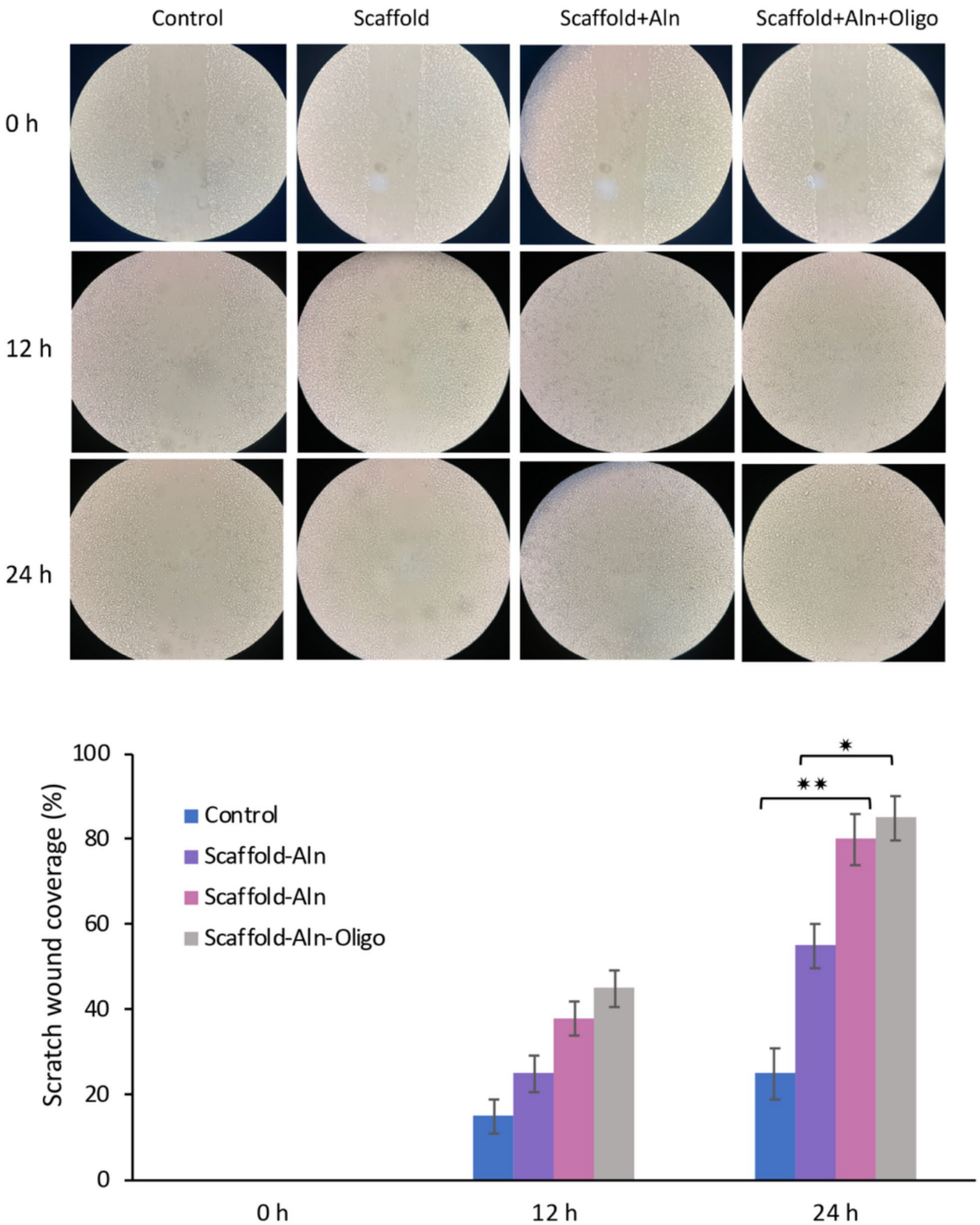

Fig. 6 The effects of different scaffolds on MG63 migration and tubular network formation. **A** Representative images of scratch wound healing assay at 0, 12, and 24 h. **B** Quantitative analysis of migrated MG63s determined by measuring the area usage of ImageJ. The control group was the cells cultured with normal medium. $p < 0.01$ (*), $p < 0.001$(**) are the percentage wound closure ± Light microscopy values ($n = 3$)

synchronized with bone regeneration timelines and controlled Aln release supports sustained osteogenesis (Wu, et al. 2015; Ammann and Rizzoli 2003).

In vitro assays revealed that Aln and oligosaccharide-loaded Aloe vera scaffolds promoted MG63 cell proliferation and migration, with minimal cytotoxicity, suggesting favorable cytocompatibility (Arslan et al. 2023; Ansari 2019; Farr and Khosla 2016). This is consistent with previous studies showing that Rosa canina-derived oligosaccharides possess antioxidant, anti-inflammatory, and differentiation-inducing properties (Khazaei et al. 2020; Sajadimajd et al. 2020). ISO 10993–4 guidelines classify materials with hemolysis rates below 5% as safe for biomedical use, further supporting scaffold compatibility (Peter et al. 2010). Additional studies on CMC composites show that additives like hydroxyapatite (HA) and bioactive glass can enhance osteogenic performance by promoting matrix mineralization and osteoblast activity (Mehrabi et al. 2024). Aln-loaded CMC hydrogels similarly prevent bone resorption and promote regeneration, with oligosaccharides contributing to the scaffold's bioactivity. Collectively, the results highlight the potential of Aloe vera-derived, Aln and oligosaccharide-loaded scaffolds as promising candidates for bone tissue engineering. Their biocompatibility, mechanical adaptability, and osteogenic support position them as viable alternatives to traditional scaffolds.

Conclusion

In this study, Aloe Vera scaffolds were decellularized and coated with CMC to enhance mechanical stability, drug release kinetics, and tissue integrity. The results indicated that this combination fostered a supportive microenvironment for cell attachment, proliferation, and differentiation. The protocol employed in the research offers a promising approach to improving bone repair outcomes for patients with bone defects or osteoporosis. The increased effectiveness of alendronate sodium through controlled release demonstrated significant potential in tissue engineering and regenerative medicine. This study contributed biocompatible and bioactive scaffolds for tissue regeneration, drug-controlled release, and improved therapeutic outcomes. Continued research and development of this strategy could transform tissue engineering and address key medical challenges related to tissue repair and regeneration.

Acknowledgements
Their search was supported by Kermanshah University of Medical Sciences, and we are very grateful for the support.

Authors' contributions
Zhila Izadi: conceptualization, supervision, project management, initial development, revision, and editing. Mahsa Abbasi and Parisa Sahami Gilan: methodology, software, validation, formal analysis. Gholamreza Bahrami and Hossein Derakhshankhah: editing, visualization. Mohammad Reza Khirehgesh, Zahra Pourmanouchehri, Maryam Zandian, Soroor Sadegh Malvajerd, and Ghazal Sanjabi: Research and data collection.

Funding
This research is supported by the University of Kermanshah Medical Sciences (Grant No. 4010017 and 4000843).

Data availability
All data generated or analyzed in this study are original and included in this article.

Declarations

Competing interests
The authors declare that they have no competing interests.

Author details
[1]Department of Chemistry, Basic of Sciences Faculty, Ilam University, Ilam, Iran. [2]Pharmaceutical Sciences Research Center, Kermanshah University of Medical Sciences, Kermanshah, Iran. [3]USERN Office, Kermanshah University of Medical Sciences, Kermanshah, Iran. [4]Nano Drug Delivery Research Center, Health Technology Institute, Kermanshah University of Medical Sciences, Kermanshah, Iran. [5]Medical Biology Research Center, Health Technology Institute, Kermanshah University of Medical Sciences, Kermanshah, Iran.

Received: 6 June 2025 Accepted: 26 August 2025
Published online: 30 September 2025

References

Ammann P, Rizzoli R (2003) Bone strength and its determinants. Osteoporos Int 14:13–18
Ansari M (2019) Bone tissue regeneration: biology, strategies and interface studies. Prog Biomater 8(4):223–237
Aoki D, Ajiro H (2017) Design of polyurethane composed of only hard main chain with oligo (ethylene glycol) units as side chain simultaneously achieved high biocompatible and mechanical properties. Macromolecules 50(17):6529–6538
Adhikari SP, Paudel A, Sharma A, Thapa B, Khanal N, Shastri N, et al (2023) Development of Decellularized Fish Skin Scaffold Decorated with Biosynthesized Silver Nanoparticles for Accelerated Burn Wound Healing. Int J Biomat 2023.
Arslan Y, Paradiso A, Celiktas N, Erdogan T, Yesil-Celiktas O, Swieszkowski W (2023) Bioinspired microstructures through decellularization of plants for tissue engineering applications. Eur Polym J 198:112415
Benslimane A, Bahlouli IM, Bekkour K, Hammiche D (2016) Thermal gelation properties of carboxymethyl cellulose and bentonite-carboxymethyl cellulose dispersions: rheological considerations. Appl Clay Sci 132:702–710
Bickhard MH (2013) Scaffolding and self-scaffolding: Central aspects of development. Children's development within social context: Psychology Press; pp. 33–52
Bilezikian JP, Raisz LG, Martin TJ (Eds.) (2008) Principles of bone biology. Academic press; pp. 362–363
Black DM, Cummings SR, Karpf DB, Cauley JA, Thompson DE, Nevitt MC et al (1996) Randomised trial of effect of alendronate on risk of fracture in women with existing vertebral fractures. Lancet 348(9041):1535–1541
Contessi Negrini N, Toffoletto N, Farè S, Altomare L (2020) Plant tissues as 3d natural scaffolds for adipose, bone and tendon tissue regeneration. Front Bioeng Biotechnol 8:723
Costa P, Lobo JMS (2001) Modeling and comparison of dissolution profiles. Eur J Pharm Sci 13(2):123–133
Desjardins P, Hansen JB, Allen M (2009) Microvolume protein concentration determination using the nanodrop 2000c spectrophotometer. JoVE (Journal of Visualized Experiments) 33:e1610
Elliott S, Robinson R (1957) The water content of bone. I. The mass of water, inorganic crystals, organic matrix, and CO2 space components in a unit volume of the dog bone. J Bone Joint Surg Am 39(1):167–188

Ensrud KE, Black DM, Palermo L, Bauer DC, Barrett-Connor E, Quandt SA et al (1997) Trreatment with alendronate prevents fractures in women at highest risk: results from the fracture intervention trial. Arch Intern Med 157(22):2617–2624
Farr JN, Khosla S (2016) Determinants of bone strength and quality in diabetes mellitus in humans. Bone 82:28–34
Gao Y, Kuok KI, Jin Y, Wang R (2019) Biomedical applications of *Aloe vera*. Crit Rev Food Sci Nutr 59(sup1):S244–S256
Gregorova A, Saha N, Kitano T, Saha P (2015) Hydrothermal effect and mechanical stress properties of carboxymethylcellulose based hydrogel food packaging. Carbohydr Polym 117:559–568
Györgyey Á, Ungvári K, Kecskeméti G, Kopniczky J, Hopp B, Oszkó A et al (2013) Attachment and proliferation of human osteoblast-like cells (MG-63) on laser-ablated titanium implant material. Mater Sci Eng, C 33(7):4251–4259
Heinze T, Pfeiffer K (1999) Studies on the synthesis and characterization of carboxymethylcellulose. Die Angew Makromol Chem 266(1):37–45
Hickey RJ, Pelling AE (2019) Cellulose biomaterials for tissue engineering. Front Bioeng Biotechnol 7:45
Hoshino K-i, Nakajima T, Matsuda T, Sakai T, Gong JP (2018) Network elasticity of a model hydrogel as a function of swelling ratio: from shrinking to extreme swelling states. Soft Matter 14(47):9693–9701
Ibrahim A, Magliulo N, Groben J, Padilla A, Akbik F, Abdel Hamid Z (2020) Hardness, an important indicator of bone quality, and the role of collagen in bone hardness. J Funct Biomater 11(4):85
Iravani S, Varma RS (2019) Plants and plant-based polymers as scaffolds for tissue engineering. Green Chem 21(18):4839–4867
Jayaramudu T, Ko H-U, Kim HC, Kim JW, Kim J (2019) Swelling behavior of polyacrylamide–cellulose nanocrystal hydrogels: swelling kinetics, temperature, and pH effects. Materials 12(13):2080
Jia W, Liu L, Li M, Zhou Y, Zhou H, Weng H et al (2022) Construction of enzyme-laden vascular scaffolds based on hyaluronic acid oligosaccharides-modified collagen nanofibers for antithrombosis and in-situ endothelialization of tissue-engineered blood vessels. Acta Biomater 153:287–298
Kadokawa J-i, Arimura T, Takemoto Y, Yamamoto K (2012) Self-assembly of amylose-grafted carboxymethyl cellulose. Carbohydr Polym 90(3):1371–1377
Khazaei M, Khazaei M, Pazhouhi M (2020) An overview of therapeutic potentials of *Rosa canina*: a traditionally valuable herb. WCRJ 7:e1580
Kim D-M, Lee H-K, Kwon Y-S, Choi Y-M (2022) Aloe vera gel conjugated cuttlefish bone graft material treated with three types of hydroxyapatite for clinical trial. J Clin Rev Case Rep 7(4):68–76
Lee J, Jung H, Park N, Park S-H, Ju JH (2019) Induced osteogenesis in plants decellularized scaffolds. Sci Rep 9(1):20194
Li M, Jia W, Zhang X, Weng H, Gu G, Chen Z (2021) Hyaluronic acid oligosaccharides modified mineralized collagen and chitosan with enhanced osteoinductive properties for bone tissue engineering. Carbohydr Polym 260:117780
Loh QL, Choong C (2013) Three-dimensional scaffolds for tissue engineering applications: role of porosity and pore size. Tissue Eng Part B Rev. https://doi.org/10.1089/ten.TEB.2012.0437
Mehrabi A, Jalise SZ, Hivechi A, Habibi S, Kebria MM, Haramshahi MA et al (2024) Evaluation of inherent properties of the carboxymethyl cellulose (<scp>CMC</scp>) for potential application in tissue engineering focusing on bone regeneration. Polym Adv Technol 35(1):e6258
Modulevsky DJ, Lefebvre C, Haase K, Al-Rekabi Z, Pelling AE (2014) Apple derived cellulose scaffolds for 3D mammalian cell culture. PLoS ONE 9(5):e97835
Mohammadinejad R, Karimi S, Iravani S, Varma RS (2016) Plant-derived nanostructures: types and applications. Green Chem 18(1):20–52
Morris VB, Nimbalkar S, Younesi M, McClellan P, Akkus O (2017) Mechanical properties, cytocompatibility and manufacturability of chitosan: PEGDA hybrid-gel scaffolds by stereolithography. Ann Biomed Eng 45:286–296
Mutra JKR, Jujjavarapu SE, Verma N (2023) Emergence of plant-based decellularized scaffolds for tissue regeneration: a review. ACS Sustain Chem Eng 11(17):6485–6497
Pan T, Song W, Cao X, Wang Y (2016) 3D bioplotting of gelatin/alginate scaffolds for tissue engineering: influence of crosslinking degree and pore architecture on physicochemical properties. J Mater Sci Technol 32(9):889–900
Parikh DV, Sachinvala ND, Calamari TA, Negulescu I (2003) Carboxymethylated Cotton for Moist Wound Healing. AATCC review 3(6)
Patel S, Choyee S, Uyanne J, Nguyen A, Lee P, Sedghizadeh P et al (2012) Non-exposed bisphosphonate-related osteonecrosis of the jaw: a critical assessment of current definition, staging, and treatment guidelines. Oral Dis 18(7):625–632
Peppas NA, Bures P, Leobandung W, Ichikawa H (2000) Hydrogels in pharmaceutical formulations. Eur J Pharm Biopharm 50(1):27–46
Peter M, Binulal N, Nair S, Selvamurugan N, Tamura H, Jayakumar R (2010) Novel biodegradable chitosan–gelatin/nano-bioactive glass ceramic composite scaffolds for alveolar bone tissue engineering. Chem Eng J 158(2):353–361
Porebski S, Bailey LG, Baum BR (1997) Modification of a CTAB DNA extraction protocol for plants containing high polysaccharide and polyphenol components. Plant Mol Biol Rep 15:8–15
Richbourg NR, Peppas NA, Sikavitsas VI (2019) Tuning the biomimetic behavior of scaffolds for regenerative medicine through surface modifications. J Tissue Eng Regen Med 13(8):1275–1293
Riswahyuli Y, Rohman A, Setyabudi FM, Raharjo S (2020) Indonesian wild honey authenticity analysis using attenuated total reflectance-fourier transform infrared (ATR-FTIR) spectroscopy combined with multivariate statistical techniques. Heliyon. https://doi.org/10.1016/j.heliyon.2020.e03662
Rodrigues EP, Torres AR, Batista JSdS, Huergo L, Hungria M (2012) A simple, economical and reproducible protein extraction protocol for proteomics studies of soybean roots. Genet Mol Biol 35:348–352
Roelofs AJ, Thompson K, Ebetino FH, Rogers MJ, Coxon FP (2010) Bisphosphonates: molecular mechanisms of action and effects on bone cells, monocytes and macrophages. Curr Pharm Des 16(27):2950–60
Rosilio V, Albrecht G, Baszkin A, Merle L (2000) Surface properties of hydrophobically modified carboxymethylcellulose derivatives. Effect of salt and proteins. Colloids and Surfaces B: Biointerfaces 19(2):163–72.
Roy S, Rhim J-W (2020) Carboxymethyl cellulose-based antioxidant and antimicrobial active packaging film incorporated with curcumin and zinc oxide. Int J Biol Macromol 148:666–676
Sajadimajd S, Bahrami G, Mohammadi B, Nouri Z, Farzaei MH, Chen JT (2020) Protective effect of the isolated oligosaccharide from *Rosa canina* in STZ-treated cells through modulation of the autophagy pathway. J Food Biochem 44(10):e13404
Shin Y, Kim D, Hu Y, Kim Y, Hong IK, Kim MS et al (2021) Ph-responsive succinoglycan-carboxymethyl cellulose hydrogels with highly improved mechanical strength for controlled drug delivery systems. Polymers 13(18):3197
Siepmann J, Peppas NA (2012) Modeling of drug release from delivery systems based on hydroxypropyl methylcellulose (HPMC). Adv Drug Deliv Rev 64:163–174
Singh G, Senapati S, Satpathi S, Behera PK, Das B, Nayak B (2022) Establishment of decellularized extracellular matrix scaffold derived from caprine pancreas as a novel alternative template over porcine pancreatic scaffold for prospective biomedical application. FASEB J 36(10):e22574
Su J-F, Huang Z, Yuan X-Y, Wang X-Y, Li M (2010) Structure and properties of carboxymethyl cellulose/soy protein isolate blend edible films crosslinked by maillard reactions. Carbohydr Polym 79(1):145–153
Surowiec RK, Allen MR, Wallace JM (2022) Bone hydration: how we can evaluate it, what can it tell us, and is it an effective therapeutic target? Bone Rep 16:101161
Tarafder S, Bose S (2014) Polycaprolactone-coated 3D printed tricalcium phosphate scaffolds for bone tissue engineering: in vitro alendronate release behavior and local delivery effect on in vivo osteogenesis. ACS Appl Mater Interfaces 6(13):9955–9965
Tohamy KM, Mabrouk M, Soliman IE, Beherei HH, Aboelnasr MA (2018) Novel alginate/hydroxyethyl cellulose/hydroxyapatite composite scaffold for bone regeneration: in vitro cell viability and proliferation of human mesenchymal stem cells. Int J Biol Macromol 112:448–460
Urciuolo A, Urbani L, Perin S, Maghsoudlou P, Scottoni F, Gjinovci A et al (2018) Decellularised skeletal muscles allow functional muscle regeneration by promoting host cell migration. Sci Rep 8(1):8398
Vyalikh A, Elschner C, Schulz MC, Mai R, Scheler U (2017) Early stages of biomineral formation—a solid-state NMR investigation of the mandibles of minipigs. Magnetochemistry 3(4):39

Von Euw S, Chan-Chang T-H-C, Paquis C, Haye B, Pehau-Arnaudet G, Babonneau F et al (2018) Organization of bone mineral: the role of mineral–water interactions. Geosciences 8(12):466
Wang Y, Dominko T, Weathers PJ (2020) Using decellularized grafted leaves as tissue engineering scaffolds for mammalian cells. In Vitro Cellular & Developmental Biology-Plant 56:765–774
Whistler R, BeMiller J (2008) Carbohydrate chemistry for food scientists. Food Aust 60(4):146–146
Wu Q, Bao J, Zhou YJ, Wang YJ, Du ZG, Shi YJ, Bu H (2015) Optimizing perfusion-decellularization methods of porcine livers for clinical-scale whole-organ bioengineering. BioMed Res Int 2015(1):785474
Yang XH, Zhu WL (2007) Viscosity properties of sodium carboxymethylcellulose solutions. Cellulose 14:409–417
Zahmati AA, Alipoor R, Shahmirzadi AR, Khori V, Abolhasani M (2017) Chemical decellularization methods and its effects on extracellular matrix. Internal Medicine and Medical Investigation Journal 2(3):76–83
Zhang W, Chen R, Xu X, Zhu L, Liu Y, Yu X et al (2022) Construction of biocompatible hydrogel scaffolds with a long-term drug release for facilitating cartilage repair. Front Pharmacol 13:922032

Publisher's Note

Springer Nature remains neutral with regard to jurisdictional claims in published maps and institutional affiliations.